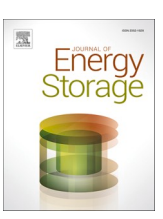
ELSEVIER

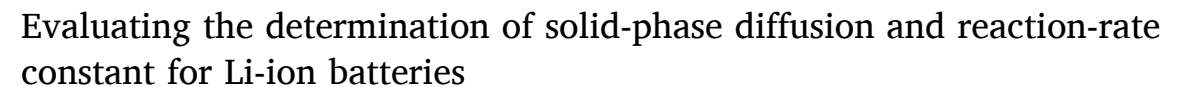
Contents lists available at ScienceDirect

Journal of Energy Storage

journal homepage: www.elsevier.com/locate/est



Research papers





- ^a Forschungszentrum Jülich GmbH, Institute of Energy Technologies (IET-1), Wilhelm-Johnen-Straße, 52428 Jülich, Germany
- ^b RWTH Aachen University, Institute of Physical Chemistry, Landoltweg 2, 52074 Aachen, Germany
- ^c High Power Research Laboratory, LLC, Idaho Falls, ID 83404, USA
- ^d Eindhoven University of Technology, P.O. Box 513, Eindhoven 5600 MB, the Netherlands
- ^e Centre for Clean Energy Technology, University of Technology Sydney, Broadway, Sydney, NSW 2007, Australia

ARTICLE INFO

Keywords:
Batteries
Battery modelling
DFN model
Galvanostatic intermittent titration technique
(GITT)
Potentiostatic intermittent titration technique
(PITT)

ABSTRACT

Physics-based models are important tools for improving Li-ion battery performance, with their accuracy heavily dependent on key parameters such as the solid-phase diffusion coefficient (D_s) and reaction-rate constant (k_0). In this work, galvanostatic intermittent titration technique (GITT) and potentiostatic intermittent titration technique (PITT) measurements were conducted on half-cells with a LiNi_{0.4}Co_{0.6}O₂ (NC46) electrode from a commercial battery. D_s and k_0 were determined using Weppner and Huggins' 1977 analytical method and physics-based optimization with the DFN model. These parameters were then implemented into the DFN model and validated under constant current with varying current densities and dynamic cycles. The combination of GITT measurements with the DFN model achieved the highest accuracy (average RMSE of 12.6 mV), while the analytical approach showed lower accuracy, especially with GITT measurements (average RMSE of 53.7 mV). Findings indicate that the widely used analytical approach in combination with GITT measurements may be unsuitable for accurately estimating D_s and k_0 due to inherent limitations and assumptions, as demonstrated here for the NC46 material. The proposed DFN model approach in combination with GITT measurements demonstrated high accuracy and versatility in determining D_s and k_0 across all lithiation levels. A sensitivity analysis further revealed that using the initial relaxation region of the GITT pulse is optimal for estimating D_s with the analytical approach.

1. Introduction

Diffusion coefficient

To improve the design, performance, and safety of LIBs, the development of reliable battery models is essential to assure the benefits of electrified transportation [1–3]. Parameterization of parameters is vital to the accuracy of the model predictions. Physics-based battery models are particularly valuable for this purpose [4]. Among these, the Doyle-Fuller-Newman (DFN) model is the model of choice due to its high accuracy in capturing the complex dynamics of battery behavior [5–8]. A critical aspect of the DFN model is its reliance on numerous parameters, which can exceed 35 in total for the full battery [9]. These parameters are typically categorized into five groups: geometric, transport, kinetic, concentration, and thermodynamic parameters.

Two key parameters that significantly influence the design, perfor-

mance, and internal state prediction of LIBs are the solid-phase diffusion coefficient (D_s) and the reaction-rate constant (k_0) . These parameters are crucial for understanding transport and kinetic processes within the battery but cannot be directly measured [9–13]. Instead, they must be determined through a combination of experimental and theoretical approaches. Notably, the values of D_s and k_0 can vary significantly depending on the electrode material, lithiation degree, or operating temperature.

A number of measurement methods have been reported in the literature for determining $D_{\rm s}$ and k_0 , including the galvanostatic intermittent titration technique (GITT) [9,11–17], potentiostatic intermittent titration technique (PITT) [16,18–22], electrochemical impedance spectroscopy (EIS) [17,22–24], and cyclic voltammetry [17,22,25,26]. Among these, GITT and PITT are particularly popular for estimating $D_{\rm s}$ and k_0 due to their simplicity and accuracy across various states of

E-mail address: l.raijmakers@fz-juelich.de (L.H.J. Raijmakers).

https://doi.org/10.1016/j.est.2025.117628

^{*} Corresponding author.

Nomenc	lature	Greek	
		$lpha_{ m a}$	Anodic charge-transfer coefficients, –
$A_{ m surf}$	Electrode surface area, m ²	$lpha_{ m c}$	Cathodic charge-transfer coefficients, –
$a_{\rm s}$	Specific interfacial surface area, m ⁻¹	δ	Thickness, m
b	Bruggeman exponent, –	$arepsilon_{ m e}$	Electrolyte volume fraction, –
$c_{ m e}$	Concentration in the electrolyte-phase, mol m ⁻³	ε_{s}	Active material volume fraction, –
$c_{\mathrm{e,0}}$	Initial electrolyte concentration, mol m ⁻³	η	Electrode overpotential, V
$c_{\rm s}$	Concentration in the solid-phase, mol m ⁻³	$\eta_{ m cc}$	Overpotentials from contact resistance, V
$c_{\rm s}^{\rm max}$	Maximum concentration in the solid-phase, mol m ⁻³	$\eta_{ m ct}$	Overpotentials from charge-transfer kinetics, V
$c_{\rm s}^{\rm surf}$	Surface concentration in the solid-phase, mol m ⁻³	$\eta_{ m e}$	Overpotentials from electrolyte dynamics, V
$D_{\rm e}$	Electrolyte-phase diffusion coefficient, m ² s ⁻¹	$\eta_{ m s}$	Overpotentials from solid-phase diffusion, V
$D_{\rm s}$	Solid-phase diffusion coefficient, m ² s ⁻¹	κ_{e}	Ionic conductivity, S m ⁻¹
F	Faraday constant, 96487 C mol ⁻¹	ν	Thermodynamic factor, –
	Mean molar activity coefficient of the electrolyte, –	$\sigma_{ extsf{s}}$	Solid-phase electronic conductivity, S m ⁻¹
f_\pm	Exchange current density, A m ⁻²	τ	Pulse time of the applied current, s
i ₀	Applied current, A	$\phi_{ m e}$	Electrolyte-phase potential, V
I _{app} ∴		$\phi_{ extsf{s}}$	Solid-phase potential, V
ĴLi	Molar ionic flux, mol m ⁻² s ⁻¹	χ	Lithiation degree, –
k_0	Reaction-rate constant, $mol^{5/2} m^{-1/2} s^{-1}$	Abbrevio	ations
L	Overall thickness of the cell, m	AEM	Advanced electrolyte model
R	Universal gas constant, 8.314 J mol ⁻¹ K ⁻¹	CC	Constant current
r	Radial position across a spherical particle, m	CEI	Cathode-electrolyte interphase
Q _{discharge}	Discharge capacity, Ah	CV	Constant voltage
Q_{pulse}	Pulse capacity, Ah	DFN	Doyle-Fuller-Newman
$R_{\rm cc}$	Contact resistance, Ω m ²	EIS	Electrochemical impedance spectroscopy
$R_{\rm ct}$	Charge-transfer resistance, Ω	EV	Electric vehicle
$R_{\rm s}$	Particle radius, m	GITT	Galvanostatic intermittent titration technique
$R_{ m f}$	Film resistance, Ω m ²	${ m Li}^+$	Li-ion
S	Active surface area, m ²	LIB	Li-ion battery
T	Temperature, K	PDE	Partial differential equation
t	Time, s	PITT	Potentiostatic intermittent titration technique
t_+^0	Transference number, –	pos	Positive electrode
U	Equilibrium potential of the electrode, V	RMSE	Root-mean-square error
V	Cell voltage, V	SEI	Solid-electrolyte interphase
$V_{ m mea}$	Measured voltage, V	sep	Separator
$V_{ m drop}^{ m dt}$	Voltage drop at time-step dt, V	WLTP	Worldwide harmonized light vehicles test procedure
x	Position across cell layers, m		
z	Charge number, –		

lithiation degree [22,27]. These two measurement methods allow the determination of both parameters with a single measurement, avoiding the need to combine with other advanced and sensitive techniques, such as EIS. Additionally, alternative techniques derived from GITT, such as the intermittent current interruption method, have been developed to reduce measurement time [28].

Estimating D_s from the aforementioned measurement methods is most commonly done using an analytical expression proposed by Weppner and Huggins in 1977 [29]. This method has been widely applied to porous LIB electrodes for parameterizing the DFN model [9,11–13]. Despite its widespread use, estimating the correct value of D_s is particularly challenging for this approach, as reported values often span several orders of magnitude, even for the same electrode composition [27]. This can be influenced on factors such as the measurement setup, determination approach, or cell design parameters (e.g., cell thickness, particle size, and active material volume fraction). Additionally, D_s is frequently treated as a concentration-independent parameter [9,13,30], although this assumption does not necessarily hold true [14,15,27,31].

The value of k_0 can be determined analytically using the voltage drop observed during measurement pulses [22]. While this method successfully eliminates the contribution from processes such as contact resistance (R_{cc}), which arise from cables and current collectors and has an

immediate effect, it does not exclude other processes contributing to the voltage drop, such as the electrolyte overpotential. Accurate application of this method requires careful consideration of these additional effects. Notably, the contribution from k_0 becomes significant only after a few hundred milliseconds to several seconds following the application of a current [32].

An alternative to applying the method of Weppner and Huggins [29] and the voltage drop for determining $D_{\rm s}$ and k_0 , lies in using the physics-based DFN modelling approach. This method involves optimizing $D_{\rm s}$ and k_0 under GITT or PITT-pulses to achieve the best fit between the simulated and measured voltage [15,33,34]. The advantage of this approach is the ability to isolate the overpotential linked to $D_{\rm s}$ and k_0 from other overpotentials in the battery. However, this approach requires accurate estimation of the other model parameters, of which the determination can be a complex and time-consuming task.

The main objective of this study is to compare and analyse various combinations of GITT and PITT measurement methods with the analytical and physics-based approaches for determining $D_{\rm s}$ and k_0 . Although these methods have been explored to some extent in previous studies [9,11–15,35], a rigorous, quantitative comparison in terms of accuracy and validation under different conditions is still lacking. This work presents a comprehensive analysis to highlight both the strengths and limitations of each method, offering a clearer understanding of

which approach is more suitable for accurate determination of D_s and k_0 . Such accuracy is essential for improving the simulation and predictive capabilities of physics-based battery models. By establishing a systematic comparison, this study underscores the importance of standardizing measurement and parameter estimation techniques in future research to ensure consistency, enhance reproducibility, and improve the overall reliability of results across the field.

The GITT and PITT measurements were performed on identical half-cells with an electrode obtained from a commercial cell. Both $D_{\rm s}$ and k_0 were obtained from the GITT and PITT measurement methods in combination with the analytical and physics-based approaches. Additionally, an optimization protocol is proposed to improve the simulation accuracy and reduce the parameter optimization time for the physics-based approaches. The simulation results using the parameters obtained from the different determination methods were validated against both constant current (CC)-discharging at various current densities and dynamic cycling, without changing and reoptimizing the parameter set. Moreover, the study includes an analysis of key assumptions related to battery parameters that influence the results obtained using the analytical approach.

2. Theoretical considerations

A typical LIB half-cell set-up, as shown in Fig. 1, consists of a positive electrode (pos), a separator (sep), and a counter electrode. The positive electrode material is made from a mixture of active electrode material, binder, and additives, coated onto a current collector, while the counter electrode is typically a Li-metal foil. The half-cell electrodes and separator are then filled with electrolyte. During discharging, positively

charged Li-ions (Li⁺) move through the electrolyte from the counter electrode to the positive electrode. Simultaneously, electrons (e⁻) flow in the same direction through the load in the external circuit. During charging, the reverse process takes place. The enlargement in Fig. 1 further illustrates the process occurring at the electrode-electrolyte interface. It is shown that Li⁺ are solvated by polar solvent molecules and move through the electrolyte along the electric field. At the surface film of the particle, Li⁺ desolvate and then migrate and diffuse through the film. The particle surface film is known as the solid-electrolyte interphase (SEI) for the negative electrode and the cathode-electrolyte interphase (CEI) for the positive electrode, which both consist of an inner and outer layer [36-40]. This film creates a resistance ($R_{\rm f}$) that impedes the movement of Li⁺ before intercalation and diffusion into the active electrode material. Over time, the film grows, influenced by factors such as state of charge, temperature (T), and lifetime, which increases R_f and leads to higher overpotentials. At the electrodeelectrolyte interface, charge-transfer reactions take place, associated with k_0 , before diffusing through the active material, a process associated with D_s .

2.1. Analytical approach for determining D_s and k_0

The diffusion of Li⁺ within the active material particles of the electrode is governed by Fick's second law of diffusion, which describes the time-dependent change in the concentration of a diffusing substance. In one dimension, this is represented as

$$\frac{\partial c_s(x,t)}{\partial t} = D_s \frac{\partial^2 c_s(x,t)}{\partial x^2} \tag{1}$$

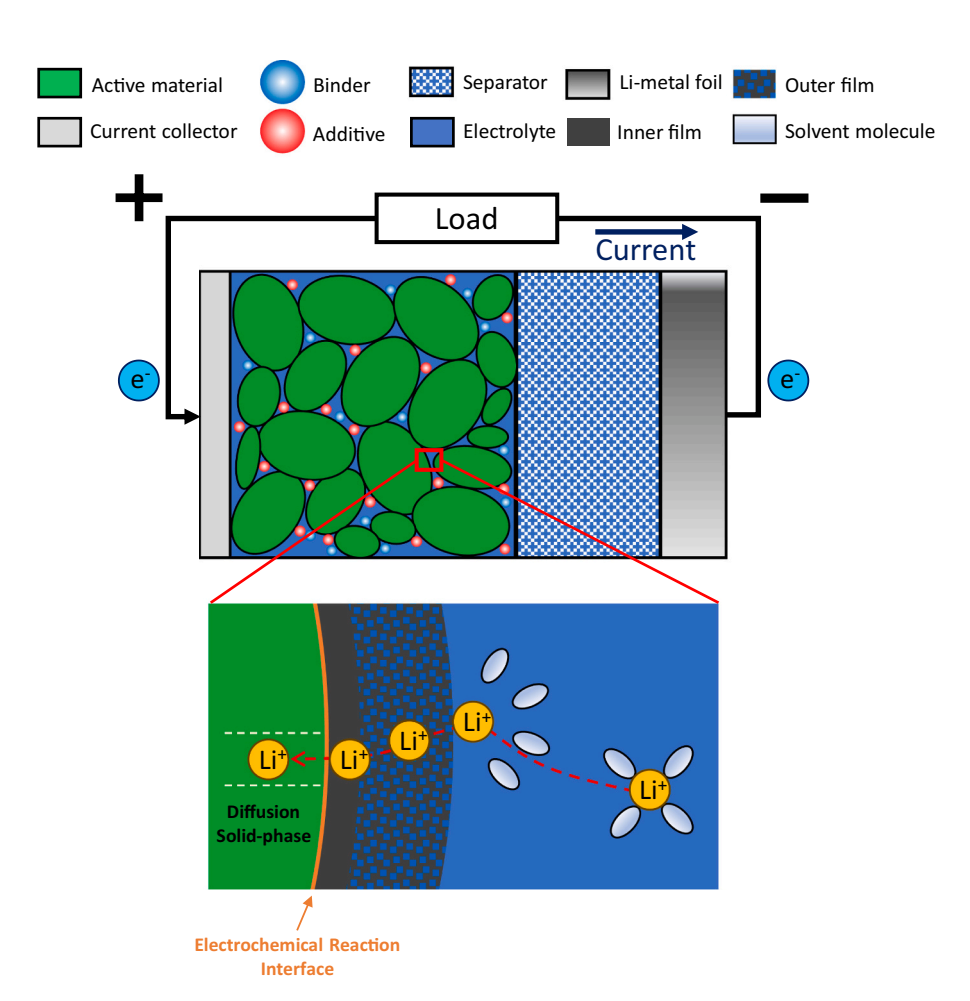


Fig. 1. Schematic representation of a LIB and the Li⁺ intercalation and diffusion processes at the electrode-electrolyte interface in a half-cell during discharge.

where c_s represents the concentration of Li⁺ in the solid-phase, t is the time, and x is the spatial coordinate along the direction of diffusion. Based on Eq. (1), Weppner and Huggins [29] developed an analytical expression to derive D_s from GITT and PITT measurements. This expression can be applied to porous electrodes for LIBs under the following assumptions [14,15,20]:

- I. Solid-phase diffusion is the only process considered in the system, while other dynamics, such as electrolyte behavior, overpotentials related to kinetics from electrochemical reactions, and aging-related overpotentials, are neglected.
- II. Diffusion is assumed to occur across a thin and dense electrode. Parameters related to the cell design, such as the electrode thickness (δ_{pos}) and active material volume fraction (ε_s) are not taken into account.
- III. Changes in electrode volume and porosity are ignored.
- IV. There are no phase transitions in the electrode.
- V. The influence of other cell components, such as the separator overpotentials, is not considered.
- VI. D_s , k_0 and cell temperature are assumed to remain constant during GITT and PITT current pulses.
- VII. The electrochemical double-layer capacitance is ignored.
- VIII. All particles in the electrode are assumed to be spherical and of uniform size.

Under assumptions I to VIII, D_s can be estimated from GITT measurements by [13,35,41,42]

$$D_s = \frac{4}{9\pi} \left(\frac{R_s}{\tau} \frac{dU}{dV/d\sqrt{\tau}} \right)^2, \tau << \frac{R_s^2}{D_s}, \tag{2}$$

and from PITT measurements by [22,43]

$$D_{\rm s} = \frac{4 R_{\rm s}^2}{\tau^2} \left(\frac{d \ln \left[I_{\rm app}(\tau) \right]}{d\tau} \right), \tau << \frac{R_{\rm s}^2}{D_{\rm s}}, \tag{3}$$

where R_s is the particle radius, τ is the duration of the applied current pulse, *U* is the equilibrium potential of the electrode, *V* is the cell voltage and I_{app} is the applied current. For obtaining D_s , the voltage profile of a GITT current pulse needs to be plotted as a function of $\sqrt{\tau}$, which is schematically shown in Fig. S1a. The slope, represented by $dV/d\sqrt{\tau}$, is then determined by fitting a linear line to the measured data. A similar approach is followed for a PITT pulse, where the current profile is plotted as $\ln(I_{app})$ versus τ . Then, $d \ln[I_{app}(\tau)]/d\tau$ represents the slope, as shown schematically in Fig. S1b. The obtained slope values can then be substituted into Eqs. (2)–(3) along with the other known parameters to calculate D_s for either a GITT or PITT pulse. Due to the influence of cables, current collectors, double-layer capacitance, charge-transfer resistance, and electrolyte, the linear fitting in this work is primarily performed from one-third of the current pulse duration to the end, assuming that only the overpotential related to D_s is dominant and influencing the voltage change during this period. The impact of assumptions I-III and the pulse fitting range on the estimated D_s results are evaluated in Section 4.3.

The charge-transfer resistance ($R_{\rm ct}$) and $R_{\rm cc}$ are assumed to be the primary contributors to the initial voltage drop after applying a current pulse [31,44], as schematically shown in Fig. S2 for both GITT (Fig. S2a) and PITT (Fig. S2b). $R_{\rm cc}$, originating from cables and current collectors, can be calculated by linearly fitting the voltage drop measured during the first 0.4 milliseconds ($V_{\rm drop}^{0.4{\rm ms}}$) of various current density pulses, as shown in Fig. S3. The fitting of $V_{\rm drop}^{0.4{\rm ms}}$ is performed with a fully charged cell because in a fully charged cell k_0 is assumed to have a high value and therefore has a reduced influence on the voltage drop during the first 0.4 milliseconds. Once $R_{\rm cc}$ is determined, $R_{\rm ct}$ can be calculated with

$$R_{\rm ct} = \frac{V_{\rm drop}^{1s}}{I_{\rm app}} - \frac{R_{\rm cc}}{A_{\rm surf}},\tag{4a}$$

where $A_{\rm surf}$ is the electrode surface area and $V_{\rm drop}^{1s}$ the voltage drop after the first second of the applied pulse, during which the overpotential contributions associated with $D_{\rm s}$ and electrolyte processes are assumed to be small and can be neglected. The one-second duration is selected as a representative value based on this assumption. The exchange current density (i_0) is then calculated by

$$i_0 = \frac{RT}{zFSR_{ct}},\tag{4b}$$

where R is the universal gas constant, F the Faraday constant and z the charge number (for LIBs, z=1). The active surface area (S), required for Eq. (4b), can be determined with

$$S = \frac{3 V_{\text{electrode } \varepsilon_{\text{S}}}}{R_{\text{S}}},\tag{4c}$$

where $V_{
m electrode}$ is the electrode volume. Finally, k_0 can be calculated with

$$k_0 = \frac{i_0}{F_{\sqrt{c_{e,0}} c_s(\chi) (c_{s,max} - c_s(\chi))}},$$
(4d)

where $c_{\rm e,0}$ is the initial electrolyte concentration and χ is the lithiation degree.

2.2. Physics-based approach for determining D_s and k_0

Fig. 2 shows a schematic representation of the relationship between the used half-cell and the DFN model. In the DFN model, the electrode is considered a collection of macroscopically homogeneous spherical particles. The DFN model captures the dynamics within the battery in two dimensions. The first dimension, referred to as the x-dimension, spans the thickness of the various cell layers at the macroscopic level, in which mass and charge transfer in both the solid and electrolyte-phases are simulated. The second dimension, known as the r-dimension,

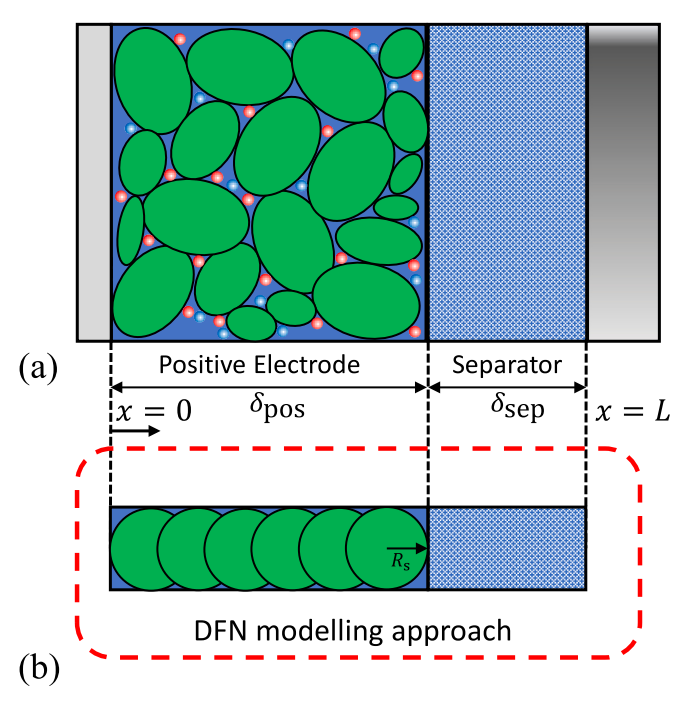


Fig. 2. Schematic illustration of a half-cell (a) and the DFN model (b).

operates on a microscopic scale and represents the particle radius. The DFN model is built on several assumptions, three of which are shared with the Weppner and Huggins [29] method (VI-VIII), described in Section 2.1, for determining $D_{\rm s}$ and k_0 using GITT and PITT measurements. To improve accuracy and eliminate the final assumption (VIII), the model can be extended to a multiple-particle DFN model [45,46]. The DFN model for a half-cell is governed by four nonlinear partial differential equations (PDEs), which are shown in Table 1. The PDEs in Eqs. (5)–(8) describe the mass and charge transfer in both the solid and electrolyte-phases of LIBs. Additionally, the Butler-Volmer equation, including the overpotential and exchange current density, is used to calculate the electrochemical reaction-rate, as shown in Eq. (9). The cell voltage is subsequently calculated using Eq. (10).

The accuracy of the model simulations using the DFN model in Table 1 depends on the model parameters, which are derived from the specific cell design and materials used. Table 2 provides a comprehensive list of parameters used in the DFN half-cell model in this work. These parameters were obtained through a combination of direct measurements, estimations, or assumptions. Electrolyte-related parameters were determined from the advanced electrolyte model (AEM) [47], which provides the relevant electrolyte properties. The properties of the separator were sourced from the manufacturer (Celgard 2325). Furthermore, both $D_{\rm S}$ and k_0 are set as unknown. The determination of these two parameters was carried out through an optimization process.

To achieve the best fit between the simulated and measured GITT or PITT pulse voltage, the parameters k_0 and D_s must be mathematically optimized. However, this process is complex. Simultaneously optimizing both parameters within a wide range can lead to local optima and extend the optimization time. To overcome these challenges, the following optimization procedure for both GITT and PITT measurements is proposed:

Table 1Governing equations of the DFN model for a half-cell.

density

Cell voltage

Li-ion concentration	$\frac{\partial c_{\rm s}(r,t)}{\partial t} = \frac{D_{\rm s}}{r^2} \frac{\partial}{\partial r} \left(r^2 \frac{\partial c_{\rm s}(r,t)}{\partial r} \right)$	(5a)
in solid-phase Boundary conditions	$\left. \frac{\partial c_s(r,t)}{\partial r} \right _{r=0} = 0, -\left. D_s \frac{\partial c_s(r,t)}{\partial r} \right _{r=R_s} = j_{\mathrm{Li}}(x,t),$	(5b)
Li-ion concentration in the	$\varepsilon_{\rm e} \frac{\partial c_{\rm e}(x,t)}{\partial t} = \frac{\partial}{\partial x} \left(D_{\rm e} \varepsilon_{\rm e}^{\rm b} \frac{\partial c_{\rm e}(x,t)}{\partial x} \right) + a_{\rm s} (1 - t_+^0) j_{\rm Li}(x,t)$	(6a)
electrolyte- phase		
Boundary conditions	$\frac{\partial c_{\rm e}(x,t)}{\partial x}\Big _{x=0} = 0, \frac{\partial c_{\rm e}(x,t)}{\partial x}\Big _{x=t} = -\frac{I_{\rm app}(t)}{A_{\rm surf}} \frac{(1-t_+^0)}{D_\rho \varepsilon_\rho^b F}$	(6b)
Specific interfacial surface area	$a_{\rm s} = \frac{3 \varepsilon_{\rm s}}{R_{\rm s}}$	(6c)
Potential in solid-phase	$\frac{\partial}{\partial x}\left(\sigma_{s}\varepsilon_{s}\frac{\partial\phi_{s}(x,t)}{\partial x}\right)=a_{s}Fj_{Li}(x,t)$	(7a)
Boundary conditions	$\sigma_{\rm s} \varepsilon_{\rm s} \frac{\partial \phi_{\rm s}(x,t)}{\partial x} \bigg _{x=0} = \frac{I_{\rm app}(t)}{A_{\rm surf}}$	(7b)
	$\left.rac{\partial \phi_{ m s}(x,t)}{\partial x} ight _{x=ar{o}_{ m pos}}=\phi_{ m s}(x,t)\left _{x=L} ight.=0$	
Potential in electrolyte-	$\frac{\partial}{\partial x}\left(\kappa_{\rm e}\varepsilon_{\rm e}^{\rm b}\frac{\partial\phi_{\rm e}(x,t)}{\partial x}+\kappa_{\rm e}\varepsilon_{\rm e}^{\rm b}\nu\frac{2RT(t)}{F}\frac{\partial{\rm In}c_{\rm e}(x,t)}{\partial x}\right)=-$	(8a)
phase Boundary conditions	$\left. egin{aligned} a_{\mathrm{s}}F_{\mathrm{Li}}(x,t) \ rac{\partial \phi_{\mathrm{e}}(x,t)}{\partial x} ight _{x=L} &= 0 \end{aligned}$	(8b)
Butler-Volmer equation	$j_{\text{Li}}(x,t) = \frac{i_0(x,t)}{F} \left(\exp\left(\alpha_a \frac{F}{RT(t)} \eta(x,t)\right) - \exp\left(\alpha_c \frac{F}{RT(t)} \eta(x,t)\right) \right)$	(9a)
Electrode overpotential	$\eta(x,t) = \phi_{s}(x,t) - \phi_{e}(x,t) - U(x,t) - R_{t}j_{Li}F$	(9b)
Exchange current	$i_0(x,t) = k_0(c_e(x,t))^{\alpha_a} \left(c_s^{max} - c_s^{surf}(x,t)\right)^{\alpha_a} \left(c_s^{surf}(x,t)\right)^{\alpha_c}$	(9c)

 $V(t) = \phi_{\rm s}(0,t) - \phi_{\rm s}(L,t) - rac{R_{
m cc}}{A_{
m surf}}I_{
m app}(t)$

Table 2
List of parameters for the DFN model.

Parameter	Positive electrode	Separator	Unit	
δ	62.5 ^a	25 ^b	μm	
$A_{ m surf}$	1.13 ^a	-	cm ²	
$\varepsilon_{ extsf{S}}$	0.55 ^d	-	-	
ε_{e}	0.21 ^a	0.39 ^b	-	
R_{s}	3.9 ^a	-	μ m	
b	1.65 ^c	1.5 ^c	_	
$\sigma_{ extsf{S}}$	75 ^a	-	${ m S}~{ m m}^{-1}$	
t_+^0	0.37 ^a	0.37^{a}	_	
$R_{\rm cc}$	0.38^{a}	_	$m\Omega$ m ²	
$lpha_{ m a}/lpha_{ m c}$	$0.5/0.5^{\circ}$	-	-	
$c_{\mathrm{e,0}}$	1000 ^b	1000^{b}	$ m mol~m^{-3}$	
$c_{\rm s}^{\rm max}$	48581 ^d	-	$ m mol~m^{-3}$	
$\chi_{100\%}/\chi_{0\%}$	1/0.26 ^d	-	-	
$D_{ m e}$	Fig. S4a ^e	Fig. S4a ^e	$m^2 s^{-1}$	
κ _e	Fig. S4b ^e	Fig. S4b ^e	${ m S}~{ m m}^{-1}$	
ν	Fig. S4c ^e	Fig. S4c ^e	-	
U	Fig. S4d ^a	-	V	

- ^a Measured.
- ^b Manufacturer.
- ^c Assumed.
- ^d Calculated.
- e AEM [47].
- a) **Obtain initial conditions:** Start by determining the initial conditions for the optimization procedure and other required parameters of the model. The initial lithiation degree for each GITT or PITT pulse is estimated based on the cumulative capacity. Next, optimize the initial k_0 by minimizing the error between the measured and simulated voltage during the first second of the pulse. Set the parameter limits to span a wide range, such as two orders of magnitude. The first second of the pulse is used for optimization because the overpotentials related to k_0 have a more significant impact on the total cell voltage at the start of the pulse compared to those from D_s . During this step, the initial value of D_s can be set to a typical value for LIB electrodes, as it has minimal influence on the results within the first second.
- b) **Optimize** D_s **and** k_0 : Optimize D_s over a broad parameter range (2–3 order of magnitude) to achieve the best fit for the full duration of the GITT or PITT pulse. Additionally, further optimize both the initial lithiation degree and k_0 by adjusting each parameter by ± 10 % and
 - $\pm\ 30$ % with respect to their initial values obtained in step a, respectively.

Procedure a-b needs to be repeated for each GITT or PITT pulse. The choice of the parameter limits during optimization depends on the material and temperature. Selecting wider limits increases computation time, as more iterations are required to achieve convergence in the optimization process. Therefore, determining the optimal lower and upper parameter limits may require trial and error. The physics-based approach to obtain D_s and k_0 is referred to as the 'DFN model' method in this work.

2.3. Model implementation and settings

Spatial and temporal discretization methods were applied to solve the PDEs described in Eqs. (5–8). The finite difference method was used to discretize Eq. (5) along the r-direction, while the finite volume method was employed for Eqs. (6)–(8) along the x-direction. Each region of the cell, including the electrodes and particles, was discretized into 15 nodes, while the separator region was discretized into 8 nodes. The resulting system of differential-algebraic equations was efficiently solved using Newton's method [48,49], with a tolerance set to 1×10^{-3} for all simulations. The simulation time step was set to 1 s, and the model

(10)

was simulated under isothermal conditions at 25 °C, consistent with the temperature at which the measurements were performed. Additionally, since this study considers beginning of life conditions, degradation mechanisms such as SEI and CEI formation were neglected. Therefore, $R_{\rm f}$ in Eq. (9b) is assumed to be 0.

3. Experimental

Measurements were performed on half-cells using coin cells (CR2032). The cell configuration included a 12 mm disc-shaped positive electrode composed of LiNi $_{0.4}$ Co $_{0.6}$ O $_2$ (NC46), a 14 mm diameter Limetal foil as the counter electrode, and an 18 mm Celgard 2325 separator (trilayer microporous membrane). The positive electrode was obtained from disassembling a fresh 2.1 Ah pouch cell (RouteJade), Fig. S4e presents a cross-sectional scanning electron microscope image of the electrode. The coin cells were filled with 50 μ L of 1 M lithium hexafluorophosphate (LiPF6) dissolved in a 50/50 (v/v) mixture of ethylene carbonate (EC) and ethyl methyl carbonate (EMC). The cells were assembled in an argon-filled glove box.

After assembly, the cells were rested for one day and then underwent two formation cycles with CC-(dis)charging at 0.18 mA cm $^{-2}$ between 4.3 V and 3 V, with a 30 min rest period between charge and discharge. This was followed by two activation cycles at 0.34 mA cm $^{-2}$ with CC and constant voltage (CV) dis(charging) between a voltage range of 4.3 V and 3 V. The cut-off current for the CV period was set to 0.04 mA cm $^{-2}$ and a 1 h rest period was applied between charge and discharge. Before measuring GITT and PITT, the cells were rested for 6 h to ensure the voltage reached a steady state. All measurements were performed in a climate chamber with the temperature set to 25 $^{\circ}$ C.

GITT and PITT discharge measurements were performed from identical starting conditions, with pulses applied between 4.3 V and 3 V. The GITT procedure included 51 pulses, each initiated by a 10 min CC-discharge at 0.34 mA cm⁻², followed by a 6 h relaxation period. For PITT measurements, potential steps of 20 mV were applied with a cut-off current limit of $3.1~\mu A~cm^{-2}$, and no relaxation period was included after each pulse. Two cells were measured for both GITT and PITT measurements of which the average D_s and k_0 values are presented in Section 4.1. Furthermore, due to the small discharge capacity observed toward the end of the PITT measurements, these values were excluded from the analysis, and only 35 pulses were used. All measurements were conducted using a commercial MPG multichannel potentiostat (Biologic ECLab, France) in combination with a commercial ICH temperature chamber (Memmert GmbH, Germany).

The use of half-cells with a Li-metal foil as the counter electrode for measurements has both advantages and disadvantages. While a three-electrode setup is sometimes employed in research [9,14,15] due to its ability to use a reference electrode that eliminates the influence of the counter electrode, this method has drawbacks. The reference electrode can introduce unwanted side effects, such as hindering ionic movement

[50] or measurement artifacts [51,52]. Moreover, three-electrode setups are more complex and require greater care to operate compared to simpler half-cells.

4. Results and discussion

4.1. Parameterization results

Fig. 3a and b shows the optimized results for D_s and k_0 as a function of lithiation degree (χ). Both D_s and k_0 are determined by applying the DFN model and the analytical approach to the GITT and PITT measurements, as shown by the four lines. The circular markers on the lines indicate the calculated values for each pulse. For the DFN model, the optimization follows the procedure outlined in steps a-b in Section 2.2, while the analytical approach applies the method detailed in Section 2.1. The root-mean-square error (RMSE) between the measured and simulated pulses from the DFN model optimization, averages around 0.35 mV for both GITT and PITT measurements. The RMSE values for each individual pulse are shown in Fig. S5.

Fig. 3a shows that the D_s values obtained using the analytical approach with GITT measurements deviate in both trend and magnitude compared to the other methods. A significant drop is observed between lithiation degrees of 0.58 and 0.69, where D_s decreases by up to three orders of magnitude relative to the average value for the rest of the lithiation degrees. This drop occurs at the lithiation degree corresponding to the plateau of the equilibrium potential, as shown in Fig. S4d, and may be attributed to a phase transition, leading to inaccurately low estimated values of D_s . As originally reported by Weppner and Huggins [29], their method is valid only until a phase change occurs (assumption IV in Section 2.1), making it less suitable for electrodes with voltage plateaus. Voltage plateaus present additional challenges for methods relying on PITT measurements, as this approach struggles to accurately capture data in flat voltage regions, thereby reducing its effectiveness under such conditions. This is evident from the yellow and purple lines in Fig. 3 between lithiation degrees of 0.58 and 0.69, where the circular markers are completely lacking for the PITT measurements. However, outside the flat potential range, both PITT methods provide reasonable D_8 values, with the results of the DFN model and analytical method in close alignment. Notably, the GITT with the DFN model does not face the same limitations as other methods. In the phase transition region, D_s values are decreasing but remain more consistent, unlike the significant drop seen with the analytical method applied to the GITT measurement.

Fig. 3a also shows the differential equilibrium potential $(dU/d\chi)$ as a function of lithiation degree, estimated from the equilibrium potential in Fig. S4d. It can be seen that for values of $dU/d\chi \approx 0$, D_s tends to be lower, whereas for higher values of $-dU/d\chi > 0$, D_s tends to be higher. In particular, this behavior aligns closely with the trends in D_s determined from GITT measurements using the DFN model, emphasizing a

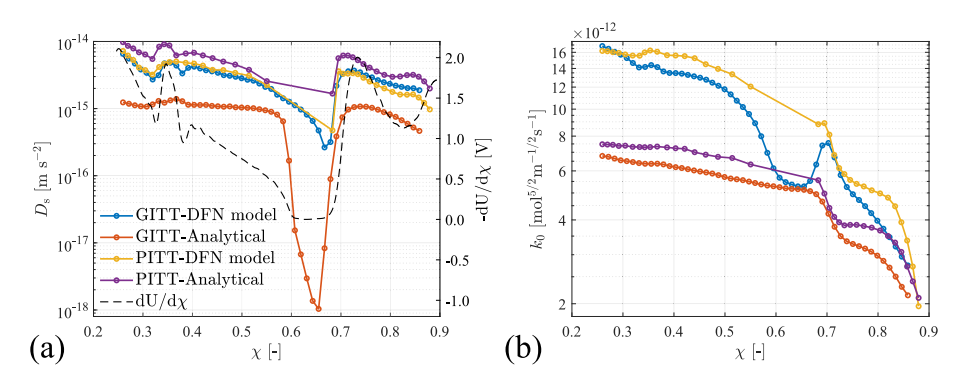


Fig. 3. Determined D_s (a) and k_0 (b) values for each measurement (GITT and PITT) and estimation method (DFN model and analytical) as a function of lithiation degree.

strong correlation between the differential equilibrium potential curve and $D_{\rm s}$.

Fig. 3b shows the optimized k_0 values, which can be broadly categorized into two groups based on the determination method, with the analytical method showing generally lower values compared to those derived from the DFN model. A notable feature is the dip in k_0 observed in the GITT measurements using the DFN model around the phase transition region (0.58 $\leq \chi \leq$ 0.69), which is less pronounced or absent in the other methods. The estimated k_0 curve follows a similar pattern to the estimated D_s curve derived using the same approach. However, k_0 shows a sharper decline at high lithiation degrees ($\chi \geq$ 0.71), a behavior not observed for D_s .

Fig. 4 shows a comparison of the GITT and PITT measurements with the DFN model simulations to provide a deeper analysis of the parameterized results. Fig. 4a and b shows the full voltage and current density profiles for the GITT and PITT measurements as a function of measurement time. In Fig. 4c and d, one pulse from each respective figure is enlarged for closer analysis by breaking it down into four distinct

overpotentials, derived from the DFN model simulations, highlighting the different contributions to the overall voltage response. In these figures, V_{mea} indicates the measured voltage. Fig. 4c shows one of the pulses during GITT measurements with an initial lithiation degree of 0.54. As can be seen in the lower plot of Fig. 4c, the overpotential ratio changes throughout the measurement duration. The simulation results indicate that the overpotential from the contact resistance (η_{cc}), associated with R_{cc} , occurs only during the period when current is applied, i. e., η_{cc} is absent during the part in which the current is zero. The average contribution of η_{cc} to the total overpotential is 7.6 % of the pulse. Overpotentials from electrolyte dynamics (η_e) are significant, contributing 32.0 % in average during the current pulse. This underscores the importance of accounting for electrolyte dynamics, contradicting assumption I of the analytical approach (Section 2.1). The contribution of η_e is initially low at the start of the pulse but increases rapidly shortly thereafter, stabilizing during the applied current and then continuing to contribute during the relaxation phase.

The overpotentials from charge-transfer kinetics (η_{ct}) and solid-

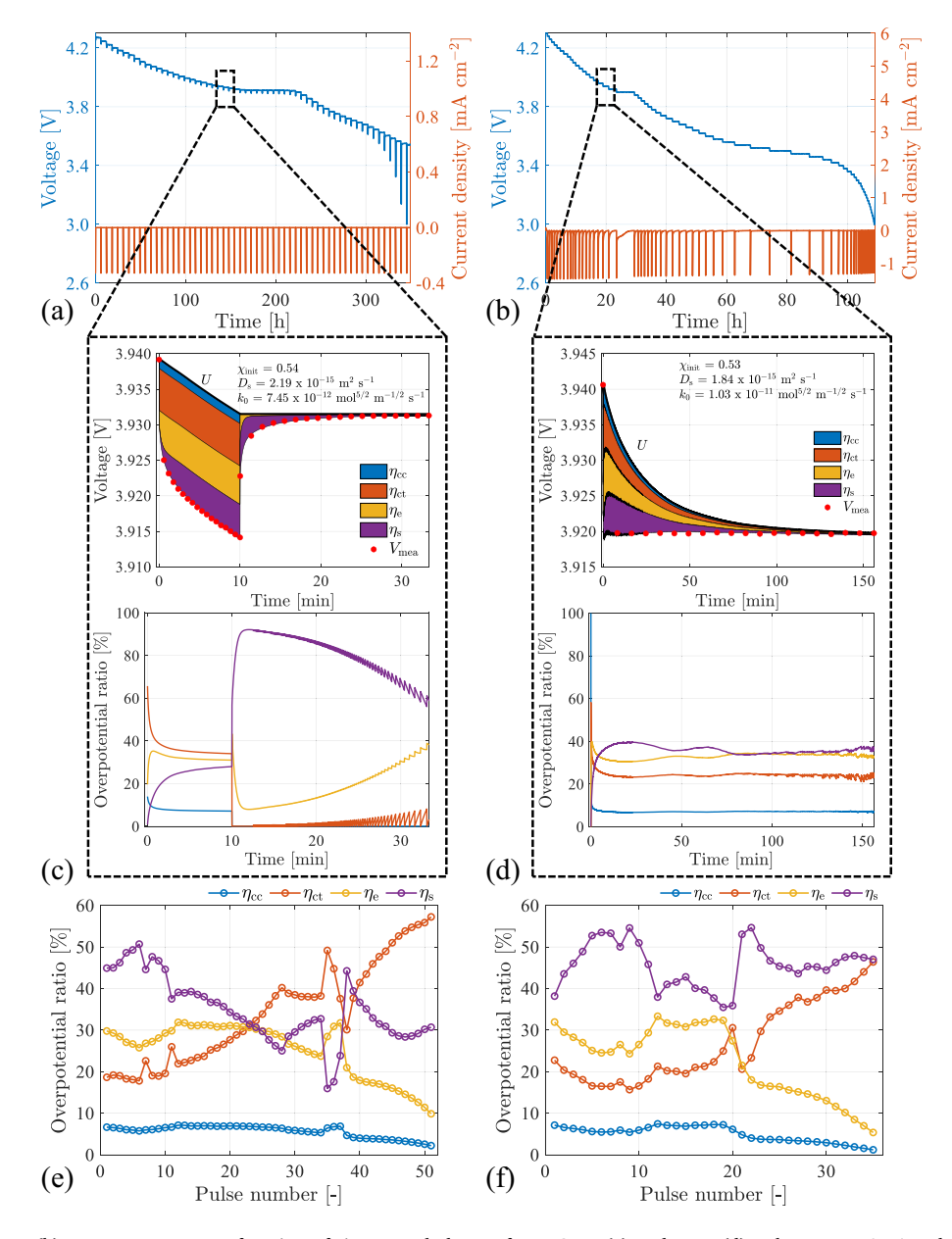


Fig. 4. GITT (a) and PITT (b) measurements as a function of time. Break-down of one GITT (c) and PITT (d) pulse at $\chi=0.54$ and $\chi=0.53$ in four distinct overpotentials with the DFN model. The total overpotential ratio during the pulses for GITT (e) and PITT (f) measurements.

phase diffusion (η_s) are associated with k_0 and D_s , respectively. The total overpotential ratio for η_{ct} during the applied current pulse averages 36.1 %, with a rapid onset at the start of the applied pulse and a quick drop to zero when entering the relaxation period. The contribution of η_s to the overpotential during the applied current pulse is 24.3 %, with a slowly increasing behavior as a function of pulse time, requiring more time to develop compared to other processes. However, η_s becomes the largest during the relaxation period due to the slow diffusion inside the solid electrode particles, requiring a relatively long time to reach equilibrium. The large discrepancy in the estimated D_s from the GITT measurements using the analytical approach compared to the other methods, shown in Fig. 3a, can be explained by the overpotential ratios shown in Fig. 4c. The analytical method assumes that only the overpotential due to D_s contributes during the applied current pulse. However, this is an inaccurate assumption, as the ratio of overpotential for η_s is not constant during the pulse, leading to incorrect estimates when fitting $dV/d\sqrt{\tau}$, as explained in Section 2.1 with help of Fig. S1. Furthermore, during the relaxation period for GITT measurements shown in the upper plot of Fig. 4c, the overpotentials gradually approach zero as the voltage reaches a steady state. This results in the overpotential ratio becoming increasingly noisy over time, primarily due to computational noise arising from the solver's set tolerance limit (Section 2.3). However, this noise has no significant impact on the results, as the overpotential values are negligible and effectively approach zero.

Fig. 4d shows the enlargement of a PITT pulse and the overpotential ratios for an initial lithiation degree of 0.53. In comparison to the GITT pulse, the overpotential ratios remain nearly constant, reaching a steady state throughout the pulse, except during the initial stage. Notably, η_s is the largest contributor compared to the other overpotentials, with an average ratio of 35.5 %, compared to 7.2 % for η_{cc} , 32.3 % for η_e , and 25.0 % for η_{ct} . These conditions aid in the fitting of $d \ln \left[I_{app}(\tau) \right] / d\tau$ for the analytical approach explained in Section 2.1, producing D_s results similar to those from the DFN model approach, as shown in Fig. 3a. Fig. S6a–d provides additional details on the GITT and PITT pulses shown in Fig. 4c and d.

To estimate k_0 , the first second of the voltage drop was used in the analytical approach. During this period, the overpotential component $\eta_{\rm ct}$ is dominant, accounting for 66 % in GITT and 58 % in PITT, as shown in Fig. S6e and f. Furthermore, it is observed that this ratio decreased over time during the applied current, while the overpotentials from $\eta_{\rm e}$ and $\eta_{\rm s}$ increases as the pulse progresses. The overpotential contribution of $\eta_{\rm cc}$ was found to be 14 % for GITT and 17 % for PITT in the first second of the pulse. The overpotential ratio for $\eta_{\rm s}$ is <1 %, far lower than $\eta_{\rm ct}$, which is needed for estimating k_0 in the analytical method, and can therefore be neglected. However, the overpotential ratio from $\eta_{\rm e}$ remains significant, contributing 20 % for GITT and 24 % for PITT measurements, and cannot be ignored. These contributions may also vary depending on the degree of lithiation.

The analytical approach assumes that the overpotential arises solely from $\eta_{\rm ct}$ and $\eta_{\rm cc}$, neglecting the contribution from $\eta_{\rm e}$. This assumption leads to lower k_0 values compared to the DFN model approach when $\eta_{\rm e}$ is significant, as shown by the two groups of lines in Fig. 3b. This demonstrates that the parameter optimization procedure outlined for the DFN model approach in Section 2.2, using the first second to estimate the initial k_0 and later reoptimizing for the full pulse with a \pm 30 % variation is valid. This approach provides flexibility in selecting the optimum time period for the pulse for determining k_0 .

Moreover, it is important to note that the individual overpotentials depend on the specific pulse selected and the degree of lithiation. Fig. 4e and f show the total overpotential ratios for various pulses during the GITT and PITT measurements. During the first half of the GITT an PITT measurement pulses, the values of η_e and η_{ct} are close to each other for both methods, but a crossover point occurs where η_{ct} increases and η_e decreases steeply. This happens at pulse number 38 for GITT and at pulse number 21 for PITT, corresponding to the same lithiation degree

point ($\chi=0.70$). Furthermore, in the voltage plateau region between pulse numbers 24 and 36 (0.58 $\leq\chi\leq0.69$) for the GITT produce, $\eta_{\rm ct}$ shows higher values compared to $\eta_{\rm e}$.

As demonstrated in Fig. 3b, the estimated k_0 values are consistent with these observations, indicating close agreement between the analytical and DFN model approaches for both GITT and PITT. The differences between these values vary between 6 % and 60 %, as shown in the full curve presented in Fig. S7. In addition, varying the voltage drop (V_{drop}^{dt}) time-period for estimating k_0 using the analytical method results in different estimated values, as shown in Fig. S8a. The analysis in Fig. S8b demonstrates that using a fixed time for the voltage drop does not produce optimum values when compared to those obtained using the DFN model approach. This indicates that estimating k_0 with the analytical method is unreliable without accounting for the influence of $\eta_{\rm e}$ or considering the possibility that the $\eta_{\rm ct}$ ratio is significantly larger than η_e by optimizing the voltage drop time-period for each pulse. It is important to note that selecting a very short time period would result in a higher overpotential contribution from the double-layer capacitance observed at the very start of a current pulse [53,54]. This effect is not accounted for in either approach, as noted in assumption VII in Section

Furthermore, η_s shows the highest average value among the overpotentials (Fig. 4e and f), with 34.9 % for GITT and 45.7 % for PITT. The observed difference in the overpotentials ratios between the GITT and PITT measurements can be attributed to the discharged capacity during the pulses (Fig. S9). GITT measurements have the advantage of maintaining a constant pulse capacity (Q_{pulse}), as shown in Fig. S9a. In contrast, PITT measurements extract uneven Q_{pulse} due to the nonlinear behavior of the electrode equilibrium potential, which becomes particularly evident from the cumulative capacity in Fig. S9b. Specifically, during or near the voltage plateau, Q_{pulse} fluctuates heavily, making it challenging to accurately estimate D_s and k_0 within that range. This limitation of PITT measurements results in reduced flexibility when evaluating other types of electrode chemistries known to feature pronounced voltage plateaus, such as Li-iron phosphate (LFP) or Li-titanium oxide (LTO). Additionally, several parameters and conditions must be carefully considered when preparing GITT or PITT measurements. Key factors include the applied current rate during the pulse, pulse duration, and relaxation time after the pulse. Applying a high current rate can lead to significant heat generation, raising the cell temperature and potentially compromising the accuracy of measurements intended for a specific temperature range.

4.2. Validation results

The D_s and k_0 values obtained from the different estimation methods and measurement techniques outlined in Section 4.1 are validated using the DFN model. The validation results, in terms of voltage profiles, are shown in Figs. 5 and 6 for CC-discharge at three currents densities and dynamic currents, respectively. The dynamic currents are based on the common Worldwide Harmonized Light Vehicles Test Procedure (WLTP), of which the current profile is shown in Fig. S10. It is important to note that no adjustments are made to the parameters during the validation process. The validation relies solely on the base parameters from Table 2 and the optimized D_s and k_0 parameters as a function of lithiation degree (Fig. 3a and b).

The CC-discharge validations were performed at current densities of 0.34, 1.00, and 1.68 mA cm $^{-2}$. Fig. 5a shows the validation results using the GITT with DFN model method (solid lines) compared to the measurements (symbols). The model demonstrates excellent accuracy across the three different current densities, maintaining an error range within ± 30 mV, except near the end of discharge. This discrepancy at the cutoff voltage can be attributed to challenges in estimating U. Fig. 5b shows the validation results for the GITT with the analytical method, which shows significant deviations between the simulated and measured data.

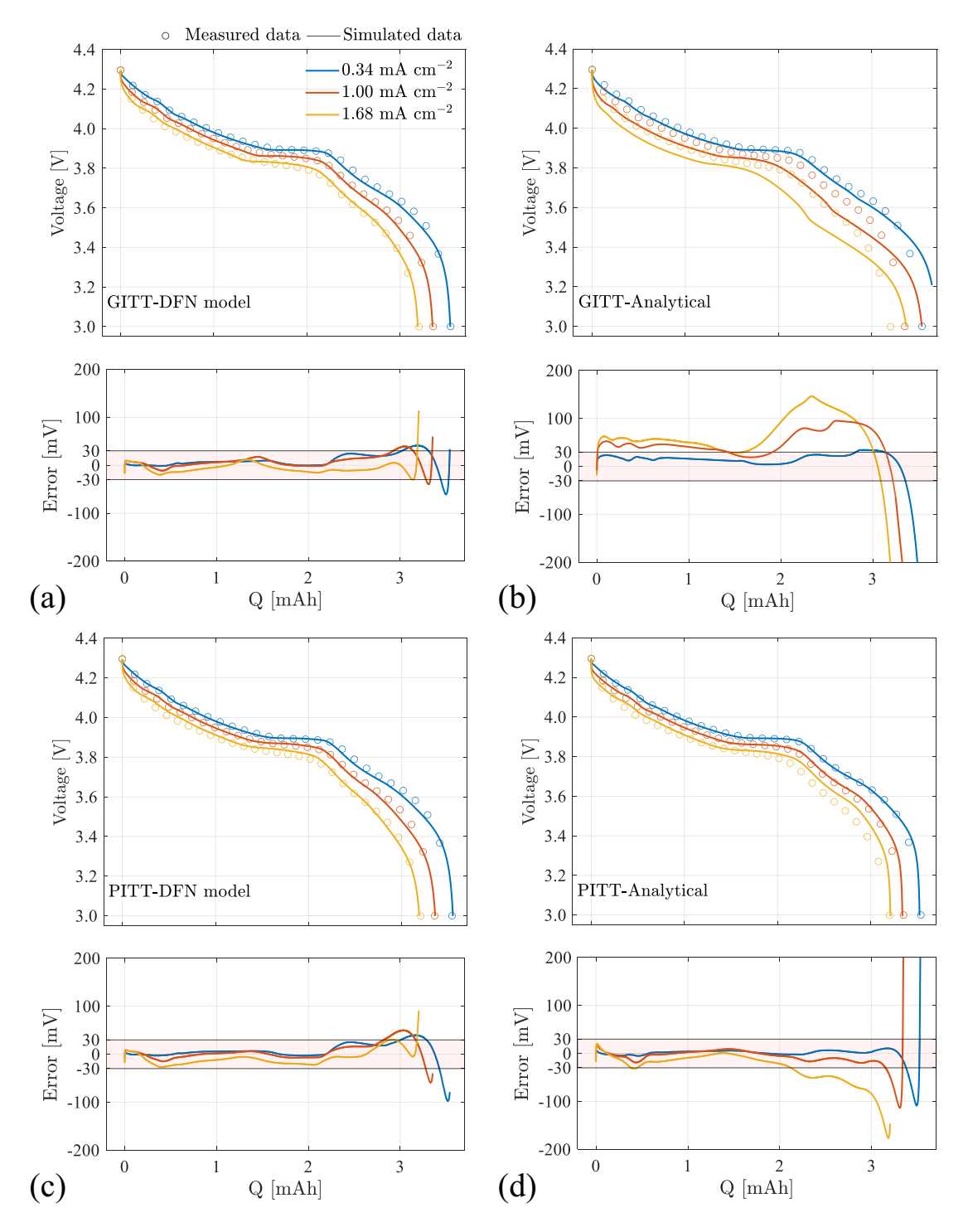


Fig. 5. Simulated data (solid lines) compared to measured data (symbols) for CC-discharging at various current densities, using different estimation methods and measurement techniques: (a) GITT-DFN model, (b) GITT-Analytical, (c) PITT-DFN model, and (d) PITT-Analytical. The error between simulated and measured data is shown below each plot.

These deviations are a result from inaccuracies in the estimation of D_s and k_0 , compared to the other three methods. This highlights the limitations of the analytical method in combination with GITT data for accurate parameter determination. Fig. 5c shows the results for the PITT with the DFN model, which also demonstrates good agreement, with most errors during the discharge period being within ± 30 mV. However, similar to the GITT with the DFN model, errors increase in the lower voltage range. Lastly, the PITT with the analytical method, shown in Fig. 5d, demonstrates improved accuracy compared to the GITT using

the analytical method. The estimated D_s aligns more closely with the values obtained using the PITT with the DFN model. However, discrepancies are primarily attributed to deviations between the two approaches in k_0 estimation, which remains less accurate compared to the DFN model approach.

To further evaluate the accuracy of the optimized D_s and k_0 parameters, a dynamic cycle based on the WLTP cycle, which involves both charging and discharging, is used, with a mean discharge current density of 1.4 mA cm⁻². Fig. 6a shows the results for the GITT measurements

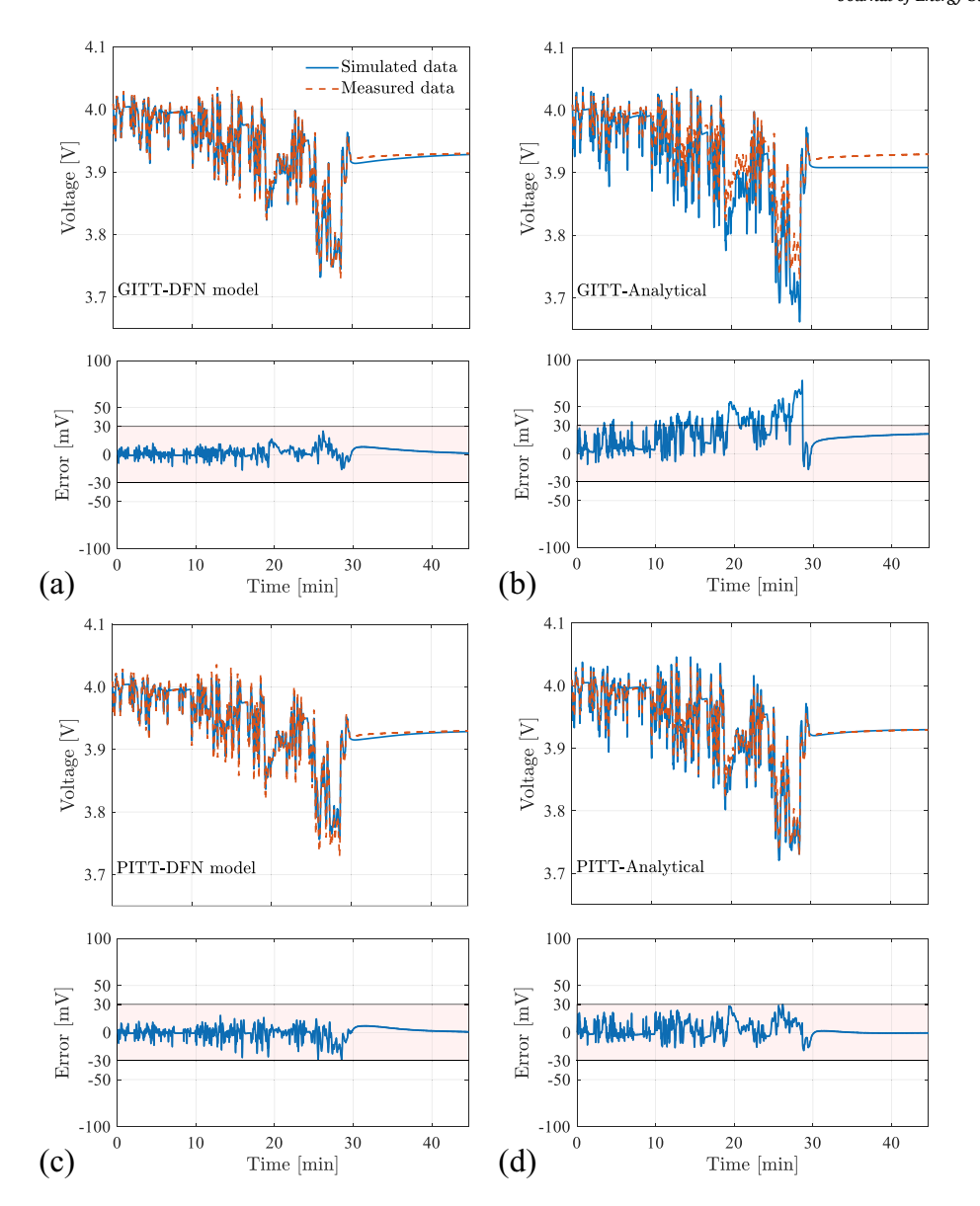


Fig. 6. Simulated data (solid lines) compared to measured data (dashed line) for a dynamic cycle, using different estimation methods and measurement techniques: (a) GITT-DFN model, (b) GITT-Analytical, (c) PITT-DFN model, and (d) PITT-Analytical. The error between simulated and measured data is shown below each plot.

with the DFN model, which, similar to the CC-discharging in Fig. 5, provides the highest accuracy among the methods used, with the error consistently remaining within ± 30 mV throughout the cycle. In contrast, Fig. 6b shows that the GITT measurements using the analytical method are the least accurate. For the PITT measurements with the DFN model, shown in Fig. 6c, the accuracy remains strong, with errors also contained within the ± 30 mV range. Lastly, Fig. 6d presents the results for the PITT measurements using the analytical approach, which, although not as accurate as the DFN model methods, still shows acceptable accuracy, keeping most errors within the ± 30 mV range.

The RMSE values for the various determination methods and conditions are summarized in Table 3. Overall, the GITT measurements combined with the DFN model achieve the lowest RMSE, ranging from 12.3 to 17.7 mV for CC-discharge at different current densities and 5.5 mV for the dynamic cycle (WLTP cycle), with an average value of 12.6 mV. The PITT measurements combined with the DFN model show the second-lowest RMSE, with an average value of 15.5 mV. The analytical methods are less accurate compared to the DFN model methods. Among the analytical methods the PITT measurement shows the best accuracy, with an average RMSE of 26.4 mV, while the GITT measurement show

Table 3RMSE values for each method across various conditions.

Method	RMSE [mV]					
	0.34 mA cm ⁻²	$\begin{array}{c} 1.00 \text{ mA} \\ \text{cm}^{-2} \end{array}$	1.68 mA cm ⁻²	Dynamic cycle	Average	
GITT-DFN model	17.7	14.8	12.3	5.5	12.6	
GITT- Analytical	45.3	63.2	80.8	25.3	53.7	
PITT-DFN model	20.7	18.4	16.7	6.1	15.5	
PITT- Analytical	24.6	26.1	46.7	8.2	26.4	

the lowest accuracy among all four methods, with an average RMSE of $53.7\ \mathrm{mV}.$

These results emphasize the importance of utilizing robust estimation approaches, such as the combination of the DFN model with GITT measurements, for accurately determining D_s and k_0 . In the case of the NC46 material studied in this work, the findings reveal that the

analytical method combined with GITT measurements, which is among the most commonly used approaches for determining $D_{\rm s}$ in the literature and is often regarded as accurate, was found to be less reliable. This observation may help explain the significant deviations in the reported $D_{\rm s}$ values for the same material across different studies. However, it should be noted that discrepancies in reported $D_{\rm s}$ values are not solely due to differences in experimental techniques or modelling assumptions, but also reflect the fact that $D_{\rm s}$ is not an intrinsic material constant. Even for the same nominal material, variability can arise due to microstructural factors such as grain boundaries, crystallographic orientation, and defects, which can lead to differences in measured diffusivities, independent of measurement or analysis technique.

4.3. Impact of cell parameters on D_s

The validation against measurement data under various operating conditions in Section 4.2 demonstrates that the DFN model combined with GITT data is the most accurate approach, particularly for capturing data during the voltage plateau. In contrast, the analytical method combined with GITT measurements reveals the lowest accuracy compared to the other methods, primarily due to its assumptions in Section 2.1. Because the analytical approach with GITT measurements is mostly used in the literature to determine D_s [9,11–13,35,41] and shows the lowest accuracy among the evaluated methods, it is chosen for further examination in this study. To investigate the influence of the method's assumptions, sensitivity analyses are performed by varying pulse current densities and electrode parameters, including electrode thickness, active material volume fraction, particle radius, and film resistance, as shown in Fig. 7a-d on the y-axis, respectively. In this analysis, a GITT pulse is applied to the DFN model with the parameters listed in Table 2. The D_s and k_0 values from Fig. 3 are used, with varying electrode parameters (δ_{pos} , ε_s , R_s and R_f) with an initial lithiation degree set to 0.37. The simulated voltage response from the GITT pulse applied to the DFN model was then used for the analytical approach to determine D_s . These D_s values are then compared by calculating the difference to the D_s from the DFN model approach, considered as the true values. The percentage differences are shown in the colour maps in

Fig. 7, with blue colours indicating small differences and yellow colours indicating large differences.

From Fig. 7a, it is evident that electrode thickness and applied current density significantly influence the estimation of D_s using the analytical method. The difference between the estimated and true values can vary from 67 % to 7.5 %, with the highest difference occurring when a thick electrode and low current density are used in this analysis. Conversely, the smallest difference is observed when a thin electrode is combined with high current density, making η_s the dominant contributor to the total overpotential. This aligns with the assumption that the analytical method was originally developed for thin-film electrodes [29]. In Fig. 7b, the effect of the electrode's active material volume fraction is examined. The largest difference, 70.3 %, occurs at a highvolume fraction with low current density. In contrast, the smallest difference, 18 %, is observed when a mid-range volume fraction is combined with medium to high current densities. Fig. 7c analyses the impact of particle radius, revealing that small particle sizes result in a high difference of up to 97 %. However, using larger particles with medium to high current densities yields the best accuracy, with the lowest difference at 0.2 %. The lower difference for the larger particles is attributed to the fact that larger particles lead to a high contribution of n_c with respect to other overpotentials, which allows for a more accurate estimation of D_s when using the analytical method. Fig. 7d illustrates the influence of film resistance. The results indicate that the resistance value itself does not cause significant differences; instead, current density is the primary factor. The largest difference, 55 % occurs at the lowest current density, while a mid-range current density reduces the difference to 25 %. The results suggest that the increase in film resistance due to battery aging does not significantly impact the estimation of D_s using the analytical method. Additionally, it is important to note that changes to the electrode design, such as thickness, active material volume fraction, or particle size, do not affect the value of D_s , as it is an intrinsic property of the electrode material. This implies that if the analytical approach was accurate, its results would align with those obtained using the DFN model approach. It is important to note that these findings are based on the parameters listed in Table 2 and are specific to the cell and material used in this study.

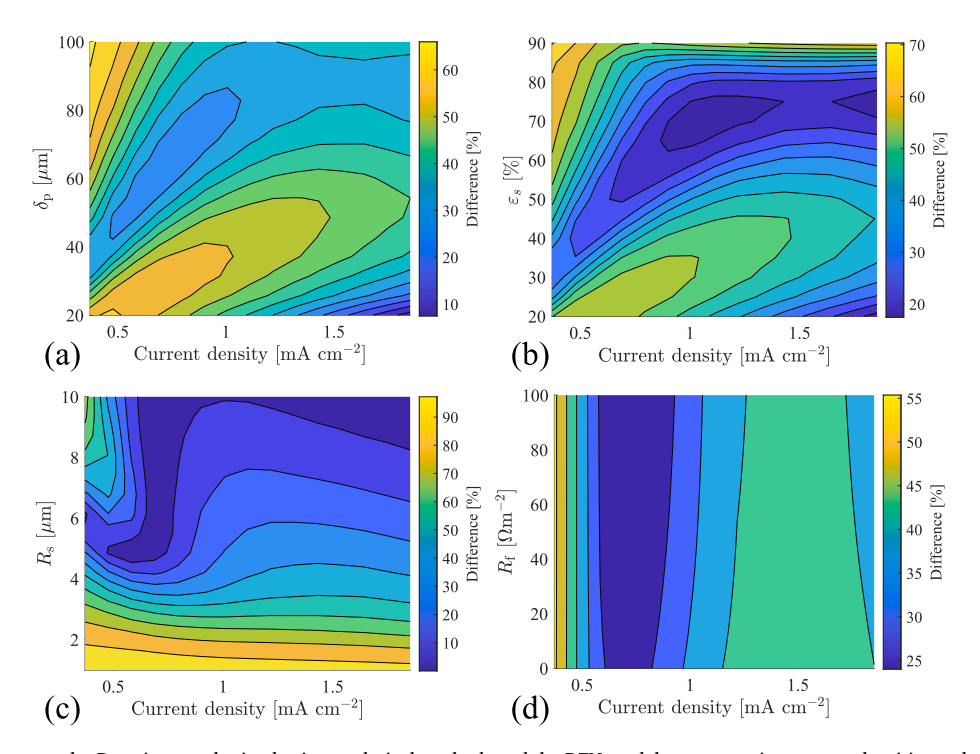


Fig. 7. The difference between the D_s estimates obtained using analytical methods and the DFN model across varying current densities and electrode parameters: (a) electrode thickness, (b) active material volume fraction, (c) particle radius, and (d) film resistance.

In addition to parameter changes, the linear fitting of $dV/d\sqrt{\tau}$ in Eq. (2) plays a significant role in determining D_s with the analytical method. In this analysis, a pulse was taken from measurement data with an initial lithiation degree of 0.37. The range for fitting $dV/d\sqrt{\tau}$ to the applied pulse was examined for different cases, as shown in Fig. 8a with the red line. Case 1, used in this work, starts from one-third to the end of the applied current pulse, as shown by the red line. Case 2 starts just after the voltage drop, and case 3 was optimized to find the best fitting range that resulted in the smallest D_s difference, starting from four-fifths of the applied pulse. Additionally, case 4 is optimized for the best fit within the relaxation region.

Fig. 8b shows the linear fit to the measured voltage for the cases 1 to 3, while Fig. 8c shows the linear fit for case 4. The differences between the estimated D_s from the analytical method using the different cases

and the estimated values from the DFN model are shown in Fig. 8d. The comparison between cases 1 to 3 reveals that the highest difference occurs in case 2, with a deviation of 60 %, while the lowest difference is 52 %. The approach used in this work (case 1) resulted in a difference of 58 %. Notably, case 4, which fits the relaxation region (from 10.7 to 14 min), results in no deviation between the analytical method and the DFN model, making it the most accurate.

Analysis of the overpotential ratios during the fitted region in case 4 reveals that η_s is the dominant contributor, with an average ratio of 91 % (Fig. S11). This dominance is discussed in more detail in Section 4.1, where the individual overpotential contributions are examined. Importantly, this finding underscores that the classic analytical method, based on fitting $dV/d\sqrt{\tau}$ during the applied current, does not provide the most accurate estimated D_s , even when using an optimized fitting range, as in

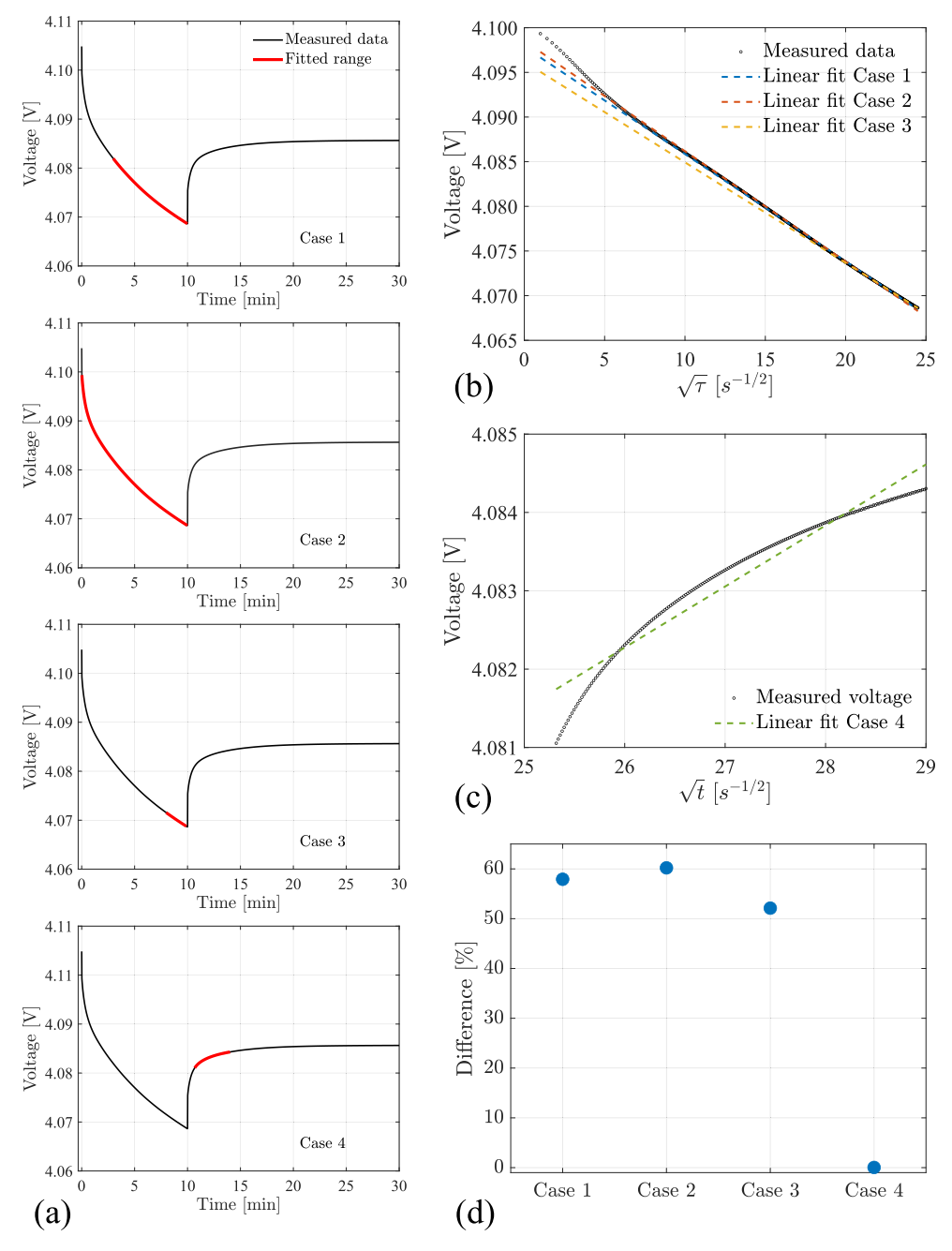


Fig. 8. Indication of four different fit range (red line) of the measured GITT pulse (black line) (a), comparison of the resulting linear fits for case 1 to 3 (b) and case 4 (c), and the differences between D_s estimates obtained from the analytical method and the DFN model method (d). (For interpretation of the references to colour in this figure legend, the reader is referred to the web version of this article.)

case 3. Instead, modifying the method to use the initial part of the relaxation region proves to be the optimal method for the analytical approach, as the overpotential associated with $D_{\rm s}$ is most dominant in that region. This is consistent with the findings of Kang et al. [55]. Moreover, the modified analytical approach, as described in case 4, can serve as a reliable initial estimate for $D_{\rm s}$ when applying the DFN model fitting. This helps to avoid the trial-and-error process described in Section 2.2 and reduces the computational demand by minimizing the number of required iterations. However, it is important to note that this method is valid only up to the point where a phase transition occurs in the electrode, when ${\rm d} U/{\rm d}\chi\approx0$.

5. Conclusions

The values of D_s and k_0 obtained from GITT and PITT measurements on NC46 material, using both analytical methods and the DFN model were compared, validated, and analyzed. Among these methods, the widely used analytical approach combined with GITT measurements was found to be the least accurate due to its underlying assumptions and inherent limitations. When the analytical method was applied with PITT measurements, the results showed more improvement in accuracy. However, due to the nature of PITT measurements, this approach is not suitable for a variety of electrodes, particularly those with voltage plateaus such as LTO and LFP. The GITT with DFN model approach emerged as the superior option, demonstrating low error in both CCdischarge at various current densities and under dynamic conditions. Furthermore, estimating k_0 was found to be inaccurate for methods with using the analytical approach, as the overpotentials from the electrolyte processes need to be taken into consideration. Applying a variable voltage drop time-period depending on the pulse improves the accuracy of the analytical approach in estimating k_0 .

Further analysis revealed that $D_{\rm S}$ estimates using the analytical method can vary significantly with changes in cell design parameters, current density, and the fitting range. Ideally, changes in electrode design parameters should not affect $D_{\rm S}$, as it is an intrinsic property of the material. Furthermore, during degradation, although the active material volume fraction decreases due to the loss of active material, $D_{\rm S}$ should theoretically remain unchanged, a consistency that the analytical method does not always maintain. Additionally, the accuracy of the analytical method is highly dependent on the fitting range of $dV/d\sqrt{\tau}$ during the pulse. However, the optimum range was found to be in the initial part of the relaxation region, as the overpotentials related to $D_{\rm S}$ are dominated.

While the simplicity of the analytical equation, which requires fewer input parameters compared to the DFN model method, is appealing, it necessitates several adjustments to cell design and fitting that are not required with the DFN model. To overcome these challenges, a more comprehensive analytical method needs to be developed, one that accounts for cell design, degradation-related parameters, and identifies the optimal fitting range. Nevertheless, the DFN model combined with the GITT method remains far more powerful and accurate, making it the preferred approach for determining both D_s and k_0 . However, the (modified) analytical and DFN model approaches can also complement each other effectively. The analytical method can offer reliable initial estimates and inform the selection of boundary limits for parameter optimization in the DFN model for determining D_s , improving accuracy while reducing computational demand. Importantly, the conclusions presented here are based on a detailed study of the NC46 material, and while the methods may be applicable more broadly, further validation is required to generalize these findings to other electrode chemistries.

CRediT authorship contribution statement

Haider Adel Ali Ali: Writing – review & editing, Writing – original draft, Visualization, Validation, Methodology, Investigation, Formal analysis, Data curation, Conceptualization. Luc H.J. Raijmakers:

Writing – review & editing, Writing – original draft, Visualization, Supervision, Resources, Project administration, Conceptualization. Anna Windmüller: Writing – review & editing. Hermann Tempel: Supervision, Project administration, Funding acquisition. Boryann Liaw: Writing – review & editing. Peter H.L. Notten: Writing – review & editing. Rüdiger-A. Eichel: Writing – review & editing, Supervision, Resources, Project administration, Funding acquisition.

Declaration of competing interest

The authors declare that they have no known competing financial interests or personal relationships that could have appeared to influence the work reported in this paper.

Acknowledgments

The authors thank their colleagues at Forschungszentrum Jülich GmbH for their great support and especially acknowledge Dr. Kudakwashe Chayambuka for his insightful discussions. This study has been developed in the LLEC::VxG and ALIBES projects, which are funded by the German Federal Ministry of Research, Technology and Space under Grant No. 03SF0628 and 13XP0530B, respectively.

Appendix A. Supplementary data

Supplementary data to this article can be found online at https://doi. org/10.1016/j.est.2025.117628.

Data availability

Data will be made available on request.

References

- J. Wen, D. Zhao, C. Zhang, An overview of electricity powered vehicles: lithium-ion battery energy storage density and energy conversion efficiency, Renew. Energy 162 (2020) 1629–1648, https://doi.org/10.1016/j.renene.2020.09.055.
- [2] J. Li, Z. Du, R.E. Ruther, S.J. An, L.A. David, K. Hays, M. Wood, N.D. Phillip, Y. Sheng, C. Mao, S. Kalnaus, C. Daniel, D.L. Wood, Toward low-cost, high-energy density, and high-power density lithium-ion batteries, JOM 69 (2017) 1484–1496, https://doi.org/10.1007/s11837-017-2404-9.
- [3] S.F. Tie, C.W. Tan, A review of energy sources and energy management system in electric vehicles, Renew. Sustain. Energy Rev. 20 (2013) 82–102, https://doi.org/ 10.1016/j.rser.2012.11.077.
- [4] J. Newman, W. Tiedemann, Porous-electrode theory with battery applications, AICHE J. 21 (1975) 25–41, https://doi.org/10.1002/aic.690210103.
- [5] K. Kumaresan, G. Sikha, R.E. White, Thermal model for a Li-ion cell, J. Electrochem. Soc. 155 (2007) A164, https://doi.org/10.1149/1.2817888.
- [6] M. Doyle, J. Newman, A.S. Gozdz, C.N. Schmutz, J.-M. Tarascon, Comparison of modeling predictions with experimental data from plastic lithium ion cells, J. Electrochem. Soc. 143 (1996) 1890, https://doi.org/10.1149/1.1836921.
- [7] V. Ramadesigan, P.W.C. Northrop, S. De, S. Santhanagopalan, R.D. Braatz, V. R. Subramanian, Modeling and simulation of lithium-ion batteries from a systems engineering perspective, J. Electrochem. Soc. 159 (2012) R31, https://doi.org/10.1149/2.018203ies
- [8] H.A.A. Ali, L.H.J. Raijmakers, K. Chayambuka, D.L. Danilov, P.H.L. Notten, R.-A. Eichel, A comparison between physics-based Li-ion battery models, Electrochim. Acta 493 (2024) 144360, https://doi.org/10.1016/j.electacta.2024.144360.
- [9] C.-H. Chen, F.B. Planella, K. O'Regan, D. Gastol, W.D. Widanage, E. Kendrick, Development of experimental techniques for parameterization of multi-scale lithium-ion battery models, J. Electrochem. Soc. 167 (2020) 080534, https://doi. org/10.1149/1945-7111/ab9050.
- [10] K. Chayambuka, M. Jiang, G. Mulder, D.L. Danilov, P.H.L. Notten, Physics-based modeling of sodium-ion batteries part I: experimental parameter determination, Electrochim. Acta 404 (2022) 139726, https://doi.org/10.1016/j. electacta.2021.139726.
- [11] M. Ecker, T.K.D. Tran, P. Dechent, S. Käbitz, A. Warnecke, D.U. Sauer, Parameterization of a physico-chemical model of a lithium-ion battery: I. Determination of parameters, J. Electrochem. Soc. 162 (2015) A1836, https://doi. org/10.1149/2.0551509jes.
- [12] J. Schmalstieg, C. Rahe, M. Ecker, D.U. Sauer, Full cell parameterization of a high-power lithium-ion battery for a physico-chemical model: Part I. Physical and electrochemical parameters, J. Electrochem. Soc. 165 (2018) A3799, https://doi.org/10.1149/2.0321816ies.
- [13] C. Schmitt, M. Gerle, D. Kopljar, K.A. Friedrich, Full parameterization study of a high-energy and high-power Li-ion cell for physicochemical models,

- J. Electrochem. Soc. 170 (2023) 070509, https://doi.org/10.1149/1945-7111/
- [14] D.W. Dees, S. Kawauchi, D.P. Abraham, J. Prakash, Analysis of the galvanostatic intermittent titration technique (GITT) as applied to a lithium-ion porous electrode, J. Power Sources 189 (2009) 263–268.
- [15] K. Chayambuka, G. Mulder, D.L. Danilov, P.H.L. Notten, Determination of state-of-charge dependent diffusion coefficients and kinetic rate constants of phase changing electrode materials using physics-based models, J. Power Sources Adv. 9 (2021) 100056, https://doi.org/10.1016/j.powera.2021.100056.
- [16] A.V. Churikov, A.V. Ivanishchev, I.A. Ivanishcheva, V.O. Sycheva, N.R. Khasanova, E.V. Antipov, Determination of lithium diffusion coefficient in LiFePO4 electrode by galvanostatic and potentiostatic intermittent titration techniques, Electrochim. Acta 55 (2010) 2939–2950, https://doi.org/10.1016/j.electacta.2009.12.079.
- [17] K. Tang, X. Yu, J. Sun, H. Li, X. Huang, Kinetic analysis on LiFePO4 thin films by CV, GITT, and EIS, Electrochim. Acta 56 (2011) 4869–4875, https://doi.org/ 10.1016/j.electacta.2011.02.119.
- [18] M.D. Levi, D. Aurbach, Diffusion coefficients of lithium ions during intercalation into graphite derived from the simultaneous measurements and modeling of electrochemical impedance and potentiostatic intermittent titration characteristics of thin graphite electrodes, J. Phys. Chem. B 101 (1997) 4641–4647, https://doi. org/10.1021/jp9701911.
- [19] S. Malifarge, B. Delobel, C. Delacourt, Guidelines for the analysis of data from the potentiostatic intermittent titration technique on battery electrodes, J. Electrochem. Soc. 164 (2017) A3925, https://doi.org/10.1149/2.1591714jes.
- [20] J. Li, F. Yang, X. Xiao, M.W. Verbrugge, Y.-T. Cheng, Potentiostatic intermittent titration technique (PITT) for spherical particles with finite interfacial kinetics, Electrochim. Acta 75 (2012) 56–61, https://doi.org/10.1016/j. electacta.2012.04.050.
- [21] J. Li, X. Xiao, F. Yang, M.W. Verbrugge, Y.-T. Cheng, Potentiostatic intermittent titration technique for electrodes governed by diffusion and interfacial reaction, J. Phys. Chem. C 116 (2012) 1472–1478, https://doi.org/10.1021/jp207919q.
- [22] H. Lee, S. Yang, S. Kim, J. Song, J. Park, C.-H. Doh, Y.-C. Ha, T.-S. Kwon, Y.M. Lee, Understanding the effects of diffusion coefficient and exchange current density on the electrochemical model of lithium-ion batteries, Curr. Opin. Electrochem. 34 (2022) 100986, https://doi.org/10.1016/j.coelec.2022.100986.
- [23] D.P. Abraham, S. Kawauchi, D.W. Dees, Modeling the impedance versus voltage characteristics of LiNi0.8Co0.15Al0.05O2, Electrochim. Acta 53 (2008) 2121–2129, https://doi.org/10.1016/j.electacta.2007.09.018.
- [24] D.R. Baker, C. Li, M.W. Verbrugge, Similarities and differences between potentialstep and impedance methods for determining diffusion coefficients of lithium in active electrode materials, J. Electrochem. Soc. 160 (2013) A1794, https://doi. org/10.1149/2.076310ies.
- [25] D. Aurbach, M.D. Levi, E. Levi, H. Teller, B. Markovsky, G. Salitra, U. Heider, L. Heider, Common electroanalytical behavior of Li intercalation processes into graphite and transition metal oxides, J. Electrochem. Soc. 145 (1998) 3024, https://doi.org/10.1149/1.1838758.
- [26] S.B. Tang, M.O. Lai, L. Lu, Li-ion diffusion in highly (0 0 3) oriented LiCoO2 thin film cathode prepared by pulsed laser deposition, J. Alloys Compd. 449 (2008) 300–303, https://doi.org/10.1016/j.jallcom.2005.12.131.
- [27] I. Santos-Mendoza, J. Vázquez-Arenas, I. González, G. Ramos-Sánchez, C. Castillo-Araiza, Revisiting electrochemical techniques to characterize the solid-state diffusion mechanism in lithium-ion batteries, Int. J. Chem. React. Eng. 17 (2019) 20180095
- [28] Y.-C. Chien, H. Liu, A.S. Menon, W.R. Brant, D. Brandell, M.J. Lacey, Rapid determination of solid-state diffusion coefficients in Li-based batteries via intermittent current interruption method, Nat. Commun. 14 (2023) 2289, https:// doi.org/10.1038/s41467-023-37989-6.
- [29] W. Weppner, R.A. Huggins, Determination of the kinetic parameters of mixed-conducting electrodes and application to the system Li3Sb, J. Electrochem. Soc. 124 (1977) 1569, https://doi.org/10.1149/1.2133112.
- [30] M. Ecker, S. Käbitz, I. Laresgoiti, D.U. Sauer, Parameterization of a physicochemical model of a lithium-ion battery: II. Model validation, J. Electrochem. Soc. 162 (2015) A1849, https://doi.org/10.1149/2.0541509jes.
- [31] A.J. Bard, L.R. Faulkner, H.S. White, Electrochemical Methods: Fundamentals and Applications, John Wiley & Sons, 2022.
- [32] W. Waag, S. Käbitz, D.U. Sauer, Experimental investigation of the lithium-ion battery impedance characteristic at various conditions and aging states and its influence on the application, Appl. Energy 102 (2013) 885–897, https://doi.org/ 10.1016/j.apenergy.2012.09.030.
- [33] K.E. Thomas, J. Newman, R.M. Darling, Mathematical modeling of Lithium batteries, in: W.A. van Schalkwijk, B. Scrosati (Eds.), Advances in Lithium-Ion Batteries, Springer US, Boston, MA, 2002, pp. 345–392, https://doi.org/10.1007/ 0-306-47508-1_13.
- [34] Y. Ye, Y. Shi, N. Cai, J. Lee, X. He, Electro-thermal modeling and experimental validation for lithium ion battery, J. Power Sources 199 (2012) 227–238.

- [35] S. Cui, Y. Wei, T. Liu, W. Deng, Z. Hu, Y. Su, H. Li, M. Li, H. Guo, Y. Duan, W. Wang, M. Rao, J. Zheng, X. Wang, F. Pan, Optimized temperature effect of Li-ion diffusion with layer distance in Li(NiMnCo)O2 cathode materials for high performance Li-ion battery, Adv. Energy Mater. 6 (2016) 1501309, https://doi.org/10.1002/aenm.201501309.
- [36] M. Mao, B. Huang, Q. Li, C. Wang, Y.-B. He, F. Kang, In-situ construction of hierarchical cathode electrolyte interphase for high performance LiNi0.8Co0.1Mn0.102/Li metal battery, Nano Energy 78 (2020) 105282, https:// doi.org/10.1016/j.nanoen.2020.105282.
- [37] B. Wu, C. Chen, D.L. Danilov, M. Jiang, L.H.J. Raijmakers, R.-A. Eichel, P.H. L. Notten, Influence of the SEI formation on the stability and lithium diffusion in Si electrodes, ACS Omega 7 (2022) 32740–32748, https://doi.org/10.1021/acsomega.2014415
- [38] Y. Zhou, M. Su, X. Yu, Y. Zhang, J.-G. Wang, X. Ren, R. Cao, W. Xu, D.R. Baer, Y. Du, O. Borodin, Y. Wang, X.-L. Wang, K. Xu, Z. Xu, C. Wang, Z. Zhu, Real-time mass spectrometric characterization of the solid–electrolyte interphase of a lithium-ion battery, Nat. Nanotechnol. 15 (2020) 224–230, https://doi.org/10.1038/s41565-019-0618-4.
- [39] S.P. Kühn, K. Edström, M. Winter, I. Cekic-Laskovic, Face to face at the cathode electrolyte interphase: from interface features to interphase formation and dynamics, Adv. Mater. Interfaces 9 (2022) 2102078, https://doi.org/10.1002/ admi.202102078.
- [40] W. Liu, P. Liu, D. Mitlin, Review of emerging concepts in SEI analysis and artificial SEI membranes for lithium, sodium, and potassium metal battery anodes, Adv. Energy Mater. 10 (2020) 2002297, https://doi.org/10.1002/aenm.202002297.
- [41] A. Nickol, T. Schied, C. Heubner, M. Schneider, A. Michaelis, M. Bobeth, G. Cuniberti, GITT analysis of lithium insertion cathodes for determining the lithium diffusion coefficient at low temperature: challenges and pitfalls, J. Electrochem. Soc. 167 (2020) 090546, https://doi.org/10.1149/1945-7111/ ab94044
- [42] Z. Shen, L. Cao, C.D. Rahn, C.-Y. Wang, Least squares galvanostatic intermittent titration technique (LS-GITT) for accurate solid phase diffusivity measurement, J. Electrochem. Soc. 160 (2013) A1842, https://doi.org/10.1149/2.084310jes.
- [43] J.M. McGraw, C.S. Bahn, P.A. Parilla, J.D. Perkins, D.W. Readey, D.S. Ginley, Li ion diffusion measurements in V205 and Li(Co1-xAlx)O2 thin-film battery cathodes, Electrochim. Acta 45 (1999) 187–196, https://doi.org/10.1016/S0013-4686(99) 00203-0.
- [44] L. Stolz, M. Winter, J. Kasnatscheew, Practical relevance of charge transfer resistance at the Li metal electrode|electrolyte interface in batteries? J. Solid State Electrochem. (2024) https://doi.org/10.1007/s10008-023-05792-4.
- [45] H.A.A. Ali, L.H.J. Raijmakers, H. Tempel, D.L. Danilov, P.H.L. Notten, R.-A. Eichel, A hybrid electrochemical multi-particle model for Li-ion batteries, J. Electrochem. Soc. 171 (2024) 110523, https://doi.org/10.1149/1945-7111/ad92dd.
- [46] T.L. Kirk, C.P. Please, S.J. Chapman, Physical modelling of the slow voltage relaxation phenomenon in lithium-ion batteries, J. Electrochem. Soc. 168 (2021) 060554. https://doi.org/10.1149/1945-7111/ac0bf7.
- [47] E.R. Logan, E.M. Tonita, K.L. Gering, J.R. Dahn, A critical evaluation of the advanced electrolyte model, J. Electrochem. Soc. 165 (2018) A3350, https://doi. org/10.1149/2.0471814jes.
- [48] Z. Khalik, M.C.F. Donkers, H.J. Bergveld, Model simplifications and their impact on computational complexity for an electrochemistry-based battery modeling toolbox, J. Power Sources 488 (2021) 229427, https://doi.org/10.1016/j. ipowsour 2020 229427
- [49] L. Xia, E. Najafi, Z. Li, H.J. Bergveld, M.C.F. Donkers, A computationally efficient implementation of a full and reduced-order electrochemistry-based model for Liion batteries, Appl. Energy 208 (2017) 1285–1296, https://doi.org/10.1016/j. apenergy.2017.09.025.
- [50] Y. Li, X. Han, X. Feng, Z. Chu, X. Gao, R. Li, J. Du, L. Lu, M. Ouyang, Errors in the reference electrode measurements in real lithium-ion batteries, J. Power Sources 481 (2021) 228933, https://doi.org/10.1016/j.jpowsour.2020.228933.
- [51] F.F. Oehler, A. Graule, S. Kücher, T. Roth, A. Adam, J. Li, E. Ronge, R. Mörtel, A. Jossen, Multi-reference electrode Lithium-ion pouch cell Design for Spatially Resolved Half-Cell Potential and Impedance Measurements, J. Electrochem. Soc. 170 (2023) 110522, https://doi.org/10.1149/1945-7111/ad048d.
- [52] L.H.J. Raijmakers, M.J.G. Lammers, P.H.L. Notten, A new method to compensate impedance artefacts for Li-ion batteries with integrated micro-reference electrodes, Electrochim. Acta 259 (2018) 517–533, https://doi.org/10.1016/j. electacta.2017.10.132.
- [53] J. Wu, Understanding the electric double-layer structure, capacitance, and charging dynamics, Chem. Rev. 122 (2022) 10821–10859, https://doi.org/ 10.1021/acs.chemrev.2c00097.
- [54] I.J. Ong, J. Newman, Double-layer capacitance in a dual Lithium ion insertion cell, J. Electrochem. Soc. 146 (1999) 4360, https://doi.org/10.1149/1.1392643.
- [55] S.D. Kang, J.J. Kuo, N. Kapate, J. Hong, J. Park, W.C. Chueh, Galvanostatic intermittent titration technique reinvented: Part II. Experiments, J. Electrochem. Soc. 168 (2021) 120503, https://doi.org/10.1149/1945-7111/ac3939.